

# Onset of intruder ground state in exotic Na isotopes and evolution of the $N = 20$ shell gap

Yutaka Utsuno,<sup>1</sup> Takaharu Otsuka,<sup>2,3,4</sup> Thomas Glasmacher,<sup>5</sup> Takahiro Mizusaki,<sup>6</sup> and Michio Honma<sup>7</sup>

<sup>1</sup>*Japan Atomic Energy Research Institute, Tokai, Ibaraki 319-1195, Japan*

<sup>2</sup>*Department of Physics, University of Tokyo, Hongo, Tokyo 113-0033, Japan*

<sup>3</sup>*Center for Nuclear Study, University of Tokyo, Hongo, Tokyo 113-0033, Japan*

<sup>4</sup>*RIKEN, Hirosawa, Wako-shi, Saitama 351-0198, Japan*

<sup>5</sup>*National Superconducting Cyclotron Laboratory and Department of Physics and Astronomy, Michigan State University, East Lansing, MI 48824, USA*

<sup>6</sup>*Institute of Natural Sciences, Senshu University,*

*Higashimita, Tama, Kawasaki, Kanagawa 214-8580, Japan*

<sup>7</sup>*Center for Mathematical Sciences, University of Aizu, Tsuruga,*

*Ikki-machi Aizu-Wakamatsu, Fukushima 965-8580, Japan*

(Dated: September 23, 2018)

The onset of intruder ground states in Na isotopes is investigated by comparing experimental data and shell-model calculations. This onset is one of the consequences of the disappearance of the  $N=20$  magic structure, and the Na isotopes are shown to play a special role in clarifying the change of this magic structure. Both the electromagnetic moments and the energy levels clearly indicate an onset of ground state intruder configurations at neutron number  $N = 19$  already, which arises only with a narrow  $N = 20$  shell gap in Na isotopes resulting from the spin-isospin dependence of the nucleon-nucleon interaction (as compared to a wider gap in stable nuclei like  $^{40}\text{Ca}$ ). It is shown why the previous report based on the mass led to a wrong conclusion.

PACS numbers: 21.60.Cs, 21.60.Ka, 27.30.+t

## I. INTRODUCTION

Amongst the most intriguing and unique features in exotic nuclei are rather significant changes from the conventional magic structure. As a result of them, the ground state of a nucleus with  $N$  or  $Z$  close to a conventional magic number is not necessarily spherical, and can be strongly deformed. Its fingerprint was first identified from extra binding energies of  $^{31,32}\text{Na}$  [1], whose origin was regarded, consistently with a Hartree-Fock calculation [2], as the dominance of strongly deformed intruder components in the ground state over the normal components. Here, normal (intruder) states imply the states comprised of shell-model configurations without (with)  $1p1h$ ,  $2p2h$  or higher excited configurations across the  $N = 20$  shell gap. Later, more direct experimental evidence of the strong deformation was found for  $^{32}\text{Mg}$  from the low excitation energy of the  $2_1^+$  state [3, 4] and the large  $B(E2; 0_1^+ \rightarrow 2_1^+)$  [5] value. Thus, the disappearance of the  $N=20$  magic structure has been established in some  $N = 20$  isotones including the recent case for  $^{30}\text{Ne}$  [6]. It still remains, however, an open question as to where the ground state changes from a normal- to an intruder-dominant configuration in the chain of isotopes, and the question as to what mechanism drives this disappearance remains. The present paper aims at presenting the resolution of these questions, as exemplified in the structure of Na isotopes.

For Na isotopes, one may expect that the onset of the intruder-dominance of the ground state lies right at  $N = 20$ , from the comparison of the experimental mass to a shell-model result within the  $sd$  shell with the USD

interaction [7]. The USD interaction has been the most frequently used interaction in the  $sd$  shell, and we shall refer to shell model calculations with this interaction in the  $sd$  shell as USD model or calculation, hereafter. A similar picture about the onset is assumed in the so-called “island of inversion” model [8, 9], where the lowest normal and the lowest intruder states are confronted without mixing between them. Although the mass (or the separation energy) often provides us with helpful information on shell structure, studies from different angles are needed before one draws definite conclusions, as we shall demonstrate. The first part of the present paper is focused upon re-examination on the dominant configuration of the ground state of Na isotopes. We perform a large-scale shell-model calculation using the Monte Carlo shell model (MCSM) [10], which is briefly described in Sec. II. In Sec. III and IV, respectively, the electromagnetic moments and the energy levels are discussed, and from such discussions the transition point from the normal- to intruder-dominant ground state is identified in the chain of Na isotopes. In Sec. V, the second part of the present paper, we discuss the mechanism of the disappearance of the magic structure, focusing upon the (effective)  $N=20$  gap between the  $sd$  and  $pf$  shells and emphasizing the special importance of the nucleus  $^{30}\text{Na}$  on this issue from a somewhat general viewpoint. We finally summarize the present study in Sec. VI.

## II. OUTLINE OF THE SHELL MODEL CALCULATION

The model space and the effective interaction used in the present study are the same as those of our previous studies [11, 12]: the valence shell consists of the full *sd*-shell orbits and two lower *pf*-shell orbits. The effective interaction is called hereafter *SDPF-M* for the sake of clarification from other interactions. The SDPF-M interaction was introduced in Ref. [11] in 1999, by combining the USD interaction [7] for the *sd* shell, the Kuo-Brown interaction [13] for the *pf* shell, and a modified Millener-Kurath interaction [14] for the cross shell. On top of this, a small but important modification was made for its monopole part [11] as we shall add some remarks later. A unique feature of the SDPF-M interaction is that the neutron shell structure, defined by the *effective single-particle energy* (ESPE), changes, as a function of the proton number, more significantly than in previous models, for instance, the “island of inversion” [8, 9]. Here, the ESPE includes mean effects from other valence nucleons on top of the usual single-particle energies with respect to the given inert core (i.e., closed shell). Therefore, the ESPE depends on shell-model interactions between valence nucleons. The present varying shell structure can be explained by the shell evolution mechanism of Ref. [15] in terms of the spin-isospin property of the effective nucleon-nucleon ( $NN$ ) interaction. The strong  $T = 0$  monopole attraction between the  $0d_{3/2}$  and the  $0d_{5/2}$  enlarges the  $N = 20$  gap, as protons occupy  $0d_{5/2}$ . Inversely, this effect diminishes towards  $Z = 8$ , ending up with a rather narrow  $N = 20$  gap and a wider  $N = 16$  gap. This shell evolution leads us to the oxygen drip line at  $N = 16$  [16, 17, 18, 19] as a result of emerging  $N = 16$  magic number [20]. The monopole part of the SDPF-M interaction was modified from that of the USD interaction so as to reproduce the oxygen drip line [11], while the resultant monopole part is closer to the G-matrix result as emphasized in [15].

In the  $N = 20$  region, as we shall illustrate, the Na isotopes give indispensable information on this shell evolution: (i) specific Na isotopes provide us with clues of a narrow  $N = 20$  shell gap, (ii) with odd  $Z$ , their ground-state properties can be directly examined by non-vanishing electromagnetic moments, and (iii) many experimental data have been recently accumulated about the mass [21], moment [22, 23],  $\gamma$ -ray spectrum and transition by the Coulomb excitation [24, 25], etc. Thus, we carry out shell-model studies on Na isotopes from  $N=16$  to 20.

Since the dimension of the Hamiltonian matrix becomes prohibitively large with the present problems, we perform a shell-model calculation by the MCSM based on the quantum Monte Carlo diagonalization (QMCD) method whose development has been described in [26, 27, 28, 29]. In the present MCSM calculation, we adopt the so-called *J-compressed* bases [29], i.e., bases generated and adopted by monitoring the energy with the full angu-

lar momentum projection. The feasibility of the MCSM calculation for odd- $A$  nuclei has been demonstrated in [12]. This method works very well for odd-odd nuclei as well.

In the present calculation, the  $E2$  matrix elements are calculated with the effective charges  $(e_p, e_n) = (1.3e, 0.5e)$  which are the same as those used in the USD model [7]. It has been confirmed that the MCSM with these effective charges excellently reproduce the  $B(E2; 0_1^+ \rightarrow 2_1^+)$  values of even-even nuclei from stable to unstable nuclei [11]. As for the effective  $M1$  operator, Brown and Wildenthal took an empirically optimum one within the USD model [30]. They found that the free-nucleon  $g$  factors give no obviously deviating magnetic moments but more quantitative agreement can be attained with the empirically optimum operator: for  $A = 28$ ,  $g_s$  is quenched by a factor 0.85, and  $g_l^p = 1.127$ ,  $g_l^n = -0.089$ ,  $g_p^p = 0.041$  and  $g_p^n = -0.35$  are used where  $l$ ,  $s$ , and  $p$  are the orbital angular momentum, the intrinsic spin, and  $\sqrt{8\pi}[Y^{(2)}(\mathbf{r}) \otimes s]^{(1)}$  operators, respectively. Recently, Honma *et al.* have presented in [31] that the spin  $g$  factor does not have to be much quenched in the full *pf*-shell model space using their newly developed interaction [31, 32]. Based on these extensive shell-model studies, the  $g$  factors are adopted, in the present MCSM calculations, so as to be rather close to the above-mentioned ones. Namely the spin part is quenched by a factor 0.9, and the other  $g$  factors are shifted from the free-nucleon values by  $\delta g_l(\text{IV}) = 0.15$  and  $\delta g_p(\text{IV}) = 0.5$  where  $g(\text{IV})$  denotes the isovector  $g$  factor defined by  $g(\text{IV}) = (g^p - g^n)/2$ .

## III. ELECTROMAGNETIC MOMENTS

The shell-model calculation described in the above section is carried out for Na isotopes from  $N = 16$  to 20. We first compare, in Fig. 1, the electric quadrupole moments and the magnetic dipole moments between the MCSM with the SDPF-M interaction and experimental data. As a reference, results from the USD model are presented, also. For the  $N = 16$  and 17 isotopes, the experimental moments [22, 23, 33] are well reproduced by both the shell-model calculations, reflecting the dominance of the *sd*-shell configurations in their ground states (see Fig. 1 (c)). It can be inferred, from the agreement with the experimental magnetic moments, that the present nucleon  $g$  factors are reasonable. At  $N = 18$ , the SDPF-M and USD calculations still give similar magnetic moments in good agreement with the experiment. On the other hand, the quadrupole moment by the SDPF-M is larger by about 30% than the USD value. Recently, a very precise measurement of the quadrupole moments for Na isotopes has been carried out by Keim *et al.* [22, 23]. The measured quadrupole moment of  $^{29}\text{Na}$  is  $8.6(3) \text{ e fm}^2$  in a good agreement with the SDPF-M prediction,  $9.1 \text{ e fm}^2$ . On the other hand, the deviation of the USD result for  $^{29}\text{Na}$  from experiment seems somewhat larger than that

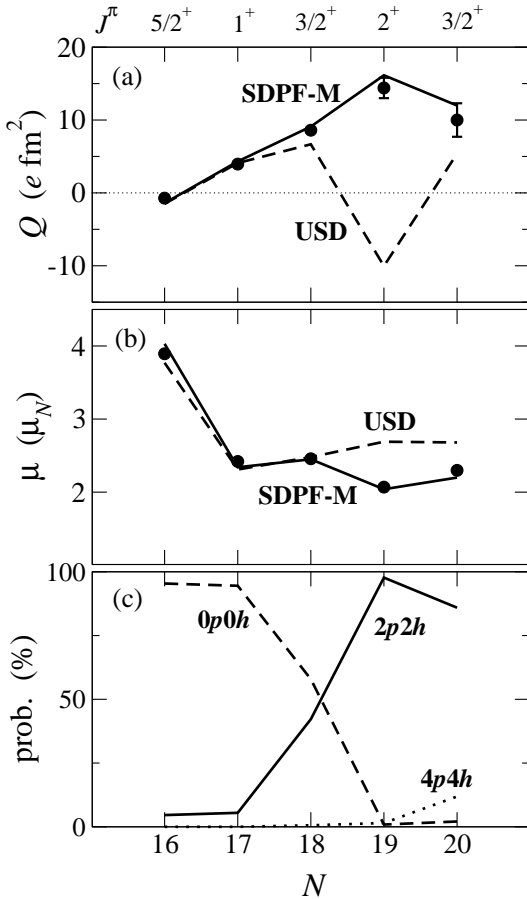


FIG. 1: (a) Electric quadrupole moments, (b) magnetic dipole moments, and (c)  $npnh$  ( $n = 0, 2, 4$ ) probabilities of the ground states of neutron-rich Na isotopes, as a function of the neutron number,  $N$ . In (a) and (b), the circles are experimental values taken from [22, 23], while the solid and the dashed lines denote, respectively, the MCSM calculation with the SDPF-M interaction and USD-model calculation.

for typical  $sd$ -shell nuclei [7]. The situation is almost unchanged if the radial wave function is replaced with the Hartree-Fock one or if the isovector effective charge is tuned [23]. It was thus suspected in [23] that the experimental quadrupole moment of  $^{29}\text{Na}$  might indicate some influence from the intruder configurations. The present MCSM calculation indeed shows, in Fig. 1 (c), the large mixing of intruder configurations by  $\sim 42\%$ , and their effects are visible in the quadrupole moment.

Unlike the cases for  $N < 19$ , in the cases of  $N = 19$  and 20, the moments cannot be reproduced by the USD model at all. Let us start with the most unstable isotope,  $^{31}\text{Na}$ . The  $^{31}\text{Na}$  nucleus ( $N = 20$ ) has been known as a typical case of the intruder dominance in the ground state [2]. Its magnetic moment was reproduced by previous shell-model calculations in a large shell-model space by Fukunishi *et al.* [35] and by Caurier *et al.* [9], supporting this picture. As shown in Fig. 1 (c), the present calculation, allowing full configurations within the va-

lence shell, confirms the intruder dominance in  $^{31}\text{Na}$  and indicates some mixing of even higher intruder configurations. Accordingly, we can reproduce not only the magnetic moment but also the quadrupole moment [22]. Note that the prediction of the energy of the first excited state of  $^{31}\text{Na}$  [12] is in agreement with the measurement by intermediate-energy Coulomb excitation [24].

We shall now move on to  $^{30}\text{Na}$  ( $N = 19$ ), which is the most crucial nucleus in this paper. The ground-state property of  $^{30}\text{Na}$  had been rather obscure so far. The observed two-neutron separation energy shows no deviation from the USD-model systematics. The ground-state spin  $J = 2$  [33] can be explained by the USD model. This is in contrast to the anomalous  $J = 3/2$  ground state in  $^{31}\text{Na}$ , which is not obtained by the USD model. The experimental magnetic moment of  $^{30}\text{Na}$   $2.083(10) \mu_N$  [33], however, deviates from the USD-model value  $2.69 \mu_N$ . This deviation seems to be somewhat larger than typical deviations in  $sd$ -shell nuclei. As Fig. 1 (b) shows, this deviation is resolved by the MCSM with the SDPF-M interaction as a consequence of the intruder ground state (see Fig. 1 (c)). As the calculated magnetic moments of  $^{30,31}\text{Na}$  can be changed only less than by 0.1  $\mu_N$  by replacing the effective  $g$  factors with the free nucleon ones, the agreement with the experiment should not be attributed to the choice of the  $g$  factors. Recently, the quadrupole moment has been measured also by Keim *et al.* [22]. This value, even its sign, turns out to be quite different from the USD prediction. Figure 1 (a) indicates that the MCSM with the SDPF-M interaction indeed reproduces this quadrupole moment, too. Therefore, the properties of the electromagnetic moments indicate that, in Na isotopes, the ground state is dominated by the intruder configurations at  $N = 19$  ( $^{30}\text{Na}$ ), and intruder configurations are substantially mixed in the ground state already at  $N = 18$ .

It may be of interest to discuss the binding energies of Na isotopes to some detail, because the USD model explains the observed trend of binding energies up to  $N=19$  rather well. Figure 2 compares the two-neutron separation energies ( $S_{2n}$ ) of Na isotopes between the experiment [21, 34] and the shell-model calculations. It can be seen that the USD gives an overall agreement with experiment as well as the MCSM calculation with the SDPF-M interaction, except for the failure by USD at  $N = 20$ . This problem at  $N = 20$  has been known for many years, as discussed in Sec. I. In fact, as previous models (see, e.g., [2, 8, 9, 12]) indicated, the shortage of the  $S_{2n}$  of  $^{31}\text{Na}$  by 1.5 MeV in the USD model is remedied by having the intruder-dominant ground state. On the other hand, the  $S_{2n}$  value at  $N = 19$  can be reproduced well by both the USD and SDPF-M, whereas their wave functions are completely different as can be seen in Fig. 1 (c). We shall now resolve this puzzle of  $^{30}\text{Na}$ .

Figure 3 (a) compares the experimental  $S_{2n}$  of  $^{30}\text{Na}$  with the calculated values by using the USD interaction and the SDPF-M interaction. With the SDPF-M interaction, we carry out two calculations, i.e., a truncated

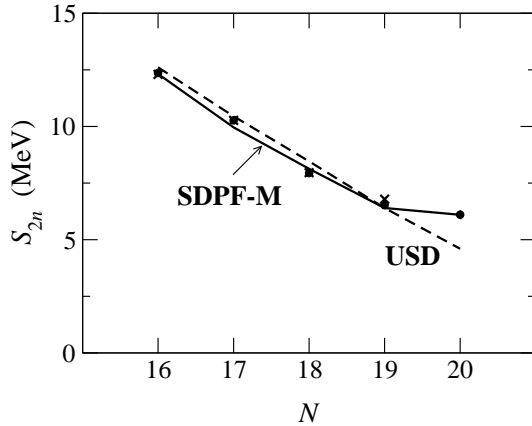


FIG. 2: Two-neutron separation energies of Na isotopes, as a function of the neutron number,  $N$ . The circles and the crosses are the experimental values taken from the mass table by Audi *et al.* [34] and a new measurement by Lunney *et al.* [21], respectively. The solid line denotes the MCSM calculation with the SDPF-M interaction, while the dashed line the USD-model calculation.

shell model within the  $sd$  shell and the full calculation. The results from the USD and the SDPF-M within the  $sd$  shell show rather different  $S_{2n}$  values of  $^{30}\text{Na}$ , despite the same model space. In order to understand this difference, the ESPE is considered as shown in Fig. 3 (b). In the SDPF-M interaction, the ESPE of the  $0d_{3/2}$  for small  $Z$  is higher than that of the USD interaction. This difference is a consequence of the shell evolution mentioned earlier, and is the largest near  $Z = 8$ , creating a new  $N = 16$  magic number. The neutron  $0d_{3/2}$  orbit is lowered as  $Z$  becomes larger, due to the strong spin-isospin dependence of the  $NN$  interaction [15]. At  $Z = 11$  (Na), this  $0d_{3/2}$  is still rather high. Thus, if the calculation is restricted to the  $sd$  shell, the SDPF-M interaction produces smaller  $S_{2n}$  than that of the USD for the nuclei where the last neutron is in the  $0d_{3/2}$ . On the other hand, the intruder configurations dominate the ground state in the full calculation by the MCSM, increasing the binding energy and making  $S_{2n}$  larger to the same extent as the USD calculation in the  $sd$  shell. Thus, almost the same separation energies can be obtained from different mechanisms, and one has to combine other physical observables to draw definite conclusions.

#### IV. ENERGY LEVELS

The energy levels of  $^{27-30}\text{Na}$  are calculated for the SDPF-M interaction by the MCSM, and are compared with both the experiment and the USD model in Fig. 4. Note that those of  $^{31}\text{Na}$  have been reported in [12], and are not included here. Although there have been just few experimental levels published so far, they provide us with important information. We shall present, with em-

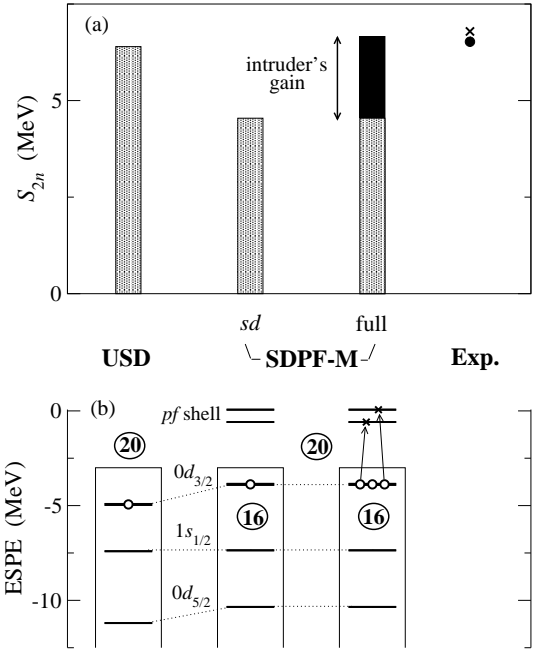


FIG. 3: (a)  $S_{2n}$  of  $^{30}\text{Na}$  compared among the shell-model calculations (with the USD interaction and the SDPF-M one) and experiment. For the SDPF-M interaction, a truncated calculation within the  $sd$  shell and the full one by the MCSM are compared, too. The circle and the cross are experimental data taken from [34] and [21], respectively. (b) Corresponding dominant neutron configurations of the ground state and the ESPE's obtained from each interaction. All the ESPE's are obtained by assuming the filling configuration.

phasis on the intruder configurations, predictions from the SDPF-M interaction, which can be some help for future experiments.

#### 1. $^{27}\text{Na}$

The USD model and the MCSM with SDPF-M give similar energy levels, and in the latter a state substantially affected by the intruder configurations does not appear low. The calculated energy levels are in good agreement with the experimental ones observed recently [36] except for the absence of the 1.725 MeV state (see Fig. 4). The agreement with the experiment confirms high predictive power of the USD interaction for near-stable nuclei. The state absent in the calculations has been tentatively assigned as the  $1/2^-$  [36]. As discussed in [36], it is unlikely that at  $N = 16$  the negative-parity state dominated by a one-neutron excitation across the  $N = 20$  gap appears low, partly because of a somewhat large gap from the  $1s_{1/2}$  to the above orbits and partly because of the strong pairing correlation in even- $N$  neutrons. If this state has a negative parity, it would involve a one-proton excitation from the  $Z = 8$  closed shell.

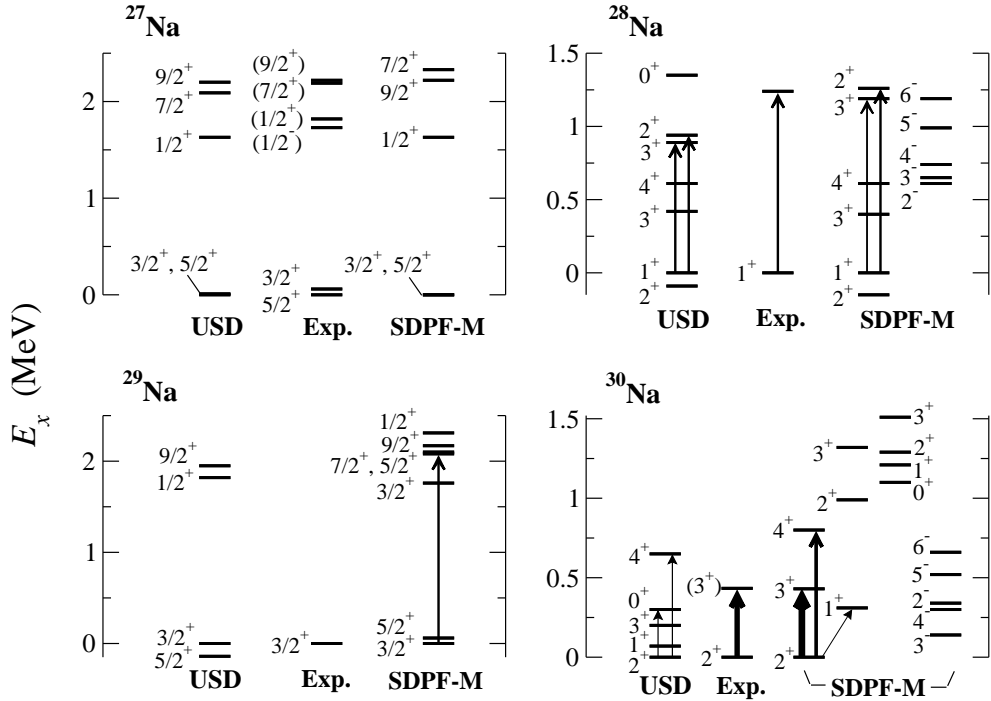


FIG. 4: Comparison of the energy levels of  $^{27-30}\text{Na}$  relative to the experimental ground state among the experiment (Exp.) and the shell-model calculations by the SDPF-M and the USD interactions. The  $E2$  strength from the ground state is illustrated by the width of the arrow. The experimental  $B(E2)$  values of  $^{28,30}\text{Na}$  and the energy levels of  $^{27}\text{Na}$  are taken from [25] and [36], respectively. For  $^{30}\text{Na}$ , the levels calculated from SDPF-M interaction are grouped into four columns; the first (second) one is  $K=2$  (1) rotational band dominated by intruder configurations, the third one represents spherical states which are basically of normal configurations, and negative-parity states are shown in the fourth column.

## 2. $^{28}\text{Na}$

The experimental ground state of  $^{28}\text{Na}$  is  $J = 1$  [33], while in the calculations the  $1_1^+$  and  $2_1^+$  states are located quite closely in energy but the  $2_1^+$  is slightly lower. The  $1_1^+$ ,  $2_1^+$ ,  $3_1^+$  and  $4_1^+$  states are dominated by the configurations consisting of a neutron  $\nu(0d_{3/2})^1$  coupled weakly to the proton  $J = 3/2^+$  or  $5/2^+$  state (see the energy levels of  $^{27}\text{Na}$ ), and are close to one another. For these states, both the shell-model calculations give similar excitation energies.

A recent Coulomb-excitation experiment by Pritychenko *et al.* [25] shows a  $\gamma$  ray at 1.24 MeV with  $B(E2) \uparrow = 54(26) e^2 \text{ fm}^4$ . The MCSM with SDPF-M gives  $B(E2; 1_1^+ \rightarrow 2_2^+) = 69 e^2 \text{ fm}^4$  and  $B(E2; 1_1^+ \rightarrow 3_2^+) = 47 e^2 \text{ fm}^4$ , either (or the sum) of which may correspond to the observed  $\gamma$  ray. On the other hand, the  $B(E2; 1_1^+ \rightarrow 2_1^+)$  and  $B(E2; 1_1^+ \rightarrow 3_1^+)$  are as small as 19 and  $27 e^2 \text{ fm}^4$ , respectively. Similar  $B(E2)$  values are obtained by the USD model, but the relevant  $2_2^+$  and  $3_2^+$  energy levels by the USD are lower by  $\sim 0.3$  MeV than those of the SDPF-M (see Fig. 4). By analyzing the occupation numbers of the wave functions, it turns out that the  $2_2^+$  and  $3_2^+$  states are mainly composed of one-neutron excitation from the  $1s_{1/2}$  to the  $0d_{3/2}$ . As the gap between these orbits is larger for the SDPF-M

interaction, those states are pushed up.

The negative-parity states are predicted to lie rather low reflecting the narrower  $N = 20$  shell gap, but there is no experimental information presently. They might be compared qualitatively to the state at 1.095 MeV in the  $N = 17$  isotope  $^{29}\text{Mg}$  which can be a negative-parity state as discussed by Baumann *et al.* [37].

## 3. $^{29}\text{Na}$

The ground state of  $^{29}\text{Na}$  is  $J = 3/2$  experimentally [33]. The calculations show very close  $3/2_1^+$  and  $5/2_1^+$  levels, and the MCSM gives the correct spin order, whereas the USD model does not (see Fig. 4). This difference is because the  $3/2_1^+$  state contains a larger mixing of the intruder configurations than the  $5/2_1^+$ . The shell-model calculations show that the  $5/2_1^+$  state is strongly connected to the ground state with  $B(E2; 3/2_1^+ \rightarrow 5/2_1^+) = 111 e^2 \text{ fm}^4$  by the USD model ( $135 e^2 \text{ fm}^4$  by the MCSM), while the  $B(E2)$  values from the ground state to the other normal-dominant low-lying states are very small. We thus point out that the Coulomb-excitation would hardly populate other excited states as far as the low-lying states are dominated by normal configurations.

In the USD model, it is predicted that there are just

$1/2_1^+$  and  $9/2_1^+$  levels around 2 MeV. Apart from these normal-dominant states, the MCSM predicts, around the same energy, low-lying  $3/2_2^+$ ,  $5/2_2^+$  and  $7/2_1^+$  states dominated by the intruder configurations. Due to the large mixing in the ground state, the  $7/2_1^+$  may be excited by the Coulomb excitation with a moderately large value,  $B(E2; 3/2_1^+ \rightarrow 7/2_1^+) = 57 e^2 \text{ fm}^4$ , as predicted by the MCSM.

#### 4. $^{30}\text{Na}$

Both the calculations succeed in reproducing the ground-state spin, but the energy levels are quite different. In the USD model, the low-lying states are composed mainly of the configurations with a neutron hole  $\nu(0d_{3/2})^{-1}$  coupled weakly to the proton  $J = 3/2$  or  $5/2$  state. The  $E2$  strength between them should then be weak as depicted in Fig. 4. On the other hand, the MCSM with SDPF-M gives the intruder-dominant ground state which is strongly deformed. Indeed, we obtain a rotational band connected by strong  $E2$  transitions: the  $E2$  matrix elements calculated by the MCSM linked to the ground state are  $B(E2; 2_1^+ \rightarrow 3_1^+) = 168 e^2 \text{ fm}^4$ ,  $B(E2; 2_1^+ \rightarrow 4_1^+) = 90 e^2 \text{ fm}^4$ , and  $Q(2_1^+) = 16 e \text{ fm}^2$ . They give rise to similar intrinsic quadrupole moments, i.e.,  $Q_0 = 58, 65$  and  $56 e \text{ fm}^2$ , respectively, by assuming  $K = 2$ . The strong  $E2$  transition has recently been measured by the Coulomb-excitation experiment by Pritychenko *et al.* [25]: from the strength of the measured  $\gamma$  ray the  $B(E2 \uparrow)$  was deduced to be  $130_{-65}^{+90} e^2 \text{ fm}^4$  consistently with the MCSM calculation. The anomalous quadrupole moment (see Fig. 1) and this large  $B(E2)$  value in  $^{30}\text{Na}$  are excellently accounted for as a result of the large prolate deformation associated with the intruder-dominant configurations.

From the viewpoint of the particle-rotor picture, the intrinsic state of the yrast band is regarded as a proton in the  $\pi[211]3/2^+$  Nilsson orbit and a neutron in the  $\nu[200]1/2^+$  coupled to a deformed  $^{28}\text{Ne}$  rotor. As a result,  $K = 1$  and  $2$  are possible as the yrast band, and the MCSM shows that the latter is favored in energy. It is of interest to point out that this feature is consistent with the so-called Gallagher-Moszkowski rule [38] that in strongly deformed nuclei the favored  $K$  is made so that the intrinsic spins of the last proton and neutron are parallel. Thus, the agreement of the ground-state spin  $J = 2$  by the MCSM is not just an accidental fortune reflecting a particular interaction matrix element, but has been conducted once the intruder configurations dominate the ground state.

The MCSM yields also the  $K = 1$  band starting at 0.31 MeV. Its  $J = 2$  and  $3$  members are calculated to lie around 1 MeV as shown in Fig. 4, while they are well mixed with the normal-dominant states. Also at  $1 \sim 1.5$  MeV excitation energy, normal-dominant spherical states, corresponding to the lowest states in the USD model, appear as shown in Fig. 4. The negative-parity

states are predicted to be rather low, dominated by the  $1p1h$  excitation across the  $N = 20$  shell gap. The competition between normal and intruder configurations in  $^{30}\text{Na}$  seems to be very intriguing, and is discussed in the next section in more detail.

## V. SHELL-GAP DEPENDENCE ON THE INTRUDER DOMINANCE

From the above discussions on the moments and the levels, it becomes evident that the transition from the normal to intruder ground state occurs fully at  $N = 19$ , after strong normal-intruder mixing already at  $N = 18$ . We shall show, in this section, that this normal-intruder transition for  $N < 20$  is particularly sensitive to the shell gap.

In general, an intruder state can be the ground state, if the energy gain due to dynamical correlations including deformation overcomes the energy loss in transcending nucleons across the shell gap. The shell gap is nothing but the difference between ESPE's of relevant orbits. The neutron ESPE changes rather gradually as a function of the neutron number, since the monopole interaction for  $T = 1$  is weak. Namely, the neutron shell gap is rather constant as a function of the neutron number. This implies that what is crucial in the transition from a normal to an intruder ground state within an isotope chain is primarily the neutron-number dependence of the correlation energy and its relative magnitude to the shell gap. Here, a good index of the correlation energy is the difference between the eigenvalue of the total Hamiltonian and the expectation value of the monopole interaction for the filling configuration.

In Fig. 5, the sources of the correlation energy are sketched schematically. Since a normal state of a (neutron) semi-magic nucleus consists of configurations shown in Fig. 5 (a), only the proton rearrangement is relevant to the correlation energy, which is generally small. On the other hand, the correlation energy is very large in the case of an intruder state composed of configurations like Fig. 5 (b), due to large numbers of particles and holes in active orbits. We note that the proton-neutron interaction produces much larger correlation energies than the interactions between like nucleons. This makes the correlation energy in Fig. 5 (b) much larger than that of Fig. 5 (a), favoring the normal-intruder inversion even with a large shell gap.

On the other hand, in the cases like Fig. 5 (c) and (d), a normal state of an open-shell nucleus has a neutron hole already. The neutron rearrangement is then possible, and strong proton-neutron two-body matrix elements contribute to the correlation energy. The intruder configurations of Fig. 5 (d) gain correlation energy similarly to the case of Fig. 5 (b). However, the difference of the correlation energy between Fig. 5 (a) and (b) is larger than that between Fig. 5 (c) and (d), because of the saturation of the correlation energy with many particles and

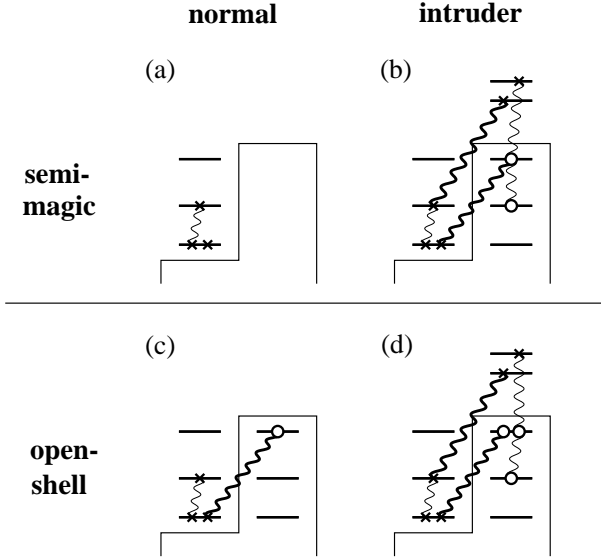


FIG. 5: Schematic sketch of the sources of the correlation energy of the intruder and the normal states of semi-magic ((a) and (b)) and open-shell ((c) and (d)) nuclei. Typical configurations for these states are shown. The proton-neutron interaction is illustrated by thick wavy lines, while the proton-proton and neutron-neutron interactions are drawn by thin wavy lines.

many holes as is the case in Fig. 5 (d). A concrete example can be found with the USD interaction: a semi-magic  $^{31}\text{Na}$  gains the correlation energy only by 1.7 MeV within the  $sd$  shell, whereas it increases to 3.7 MeV for  $^{30}\text{Na}$  and further to 7.2 MeV for  $^{29}\text{Na}$ . The correlation energy of intruder states increases more slowly due to the saturation as mentioned just above. This implies that the intruder dominance in  $N < 20$  nuclei becomes less favored as  $N$  goes down from 20. Hence, if the normal-intruder inversion still occurs, it should be due to a narrower shell gap. We shall present a more detailed account on this point now.

The SDPF-M interaction indeed gives a narrow  $N = 20$  shell gap ( $\sim 3$  MeV) for Na isotopes. Note that it still reproduces the large gap ( $\sim 6$  MeV) of  $^{40}\text{Ca}$ , owing to its monopole property. We now demonstrate how such a narrow gap of Na isotopes plays a crucial role in the intruder dominance in  $^{30}\text{Na}$ , by means of a simulation based on the argument just above. Namely, we vary the shell gap from the value given by the SDPF-M interaction to larger values, to see what happens. This can be done by changing the monopole interaction between the  $0d_{5/2}$  and the  $0d_{3/2}$  as

$$\delta V_{0d_{5/2},0d_{3/2}}^{T=1,0}(x) = -0.3x, +0.7x \text{ MeV}, \quad (1)$$

where  $V_{ij}^T$  denotes the monopole interaction between  $i$  and  $j$  orbits with isospin coupled to  $T$  [11]. The parameter  $x$  is to control the ESPE:  $x = 0$  represents the situation with the SDPF-M interaction as a starting point.

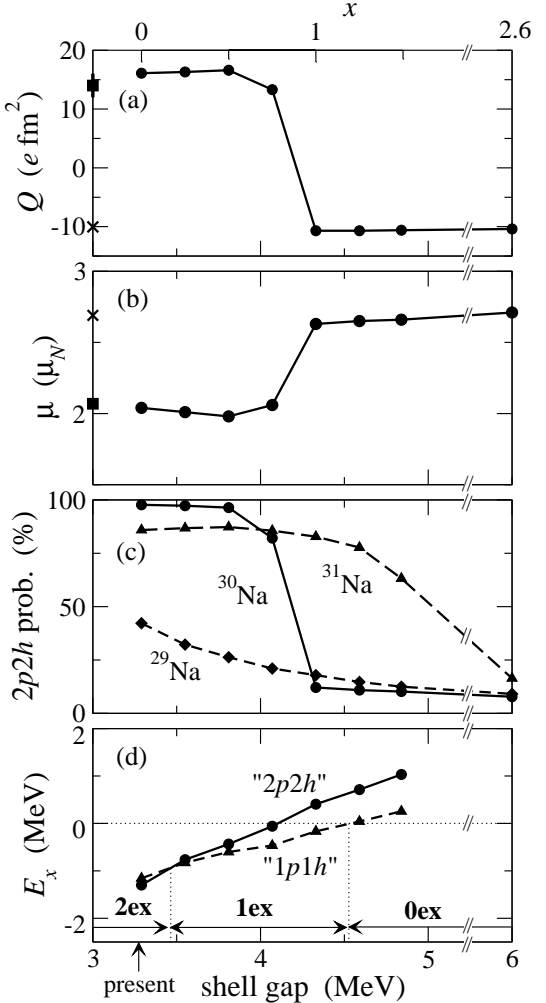


FIG. 6: (a) Quadrupole moment and (b) magnetic moment of  $^{30}\text{Na}$  as a function of the  $N = 20$  shell gap (controlled by a parameter  $x$  in Eq. (1)). The experimental [22, 23] and USD-model ones are denoted by the squares and crosses, respectively. (c)  $2p2h$  probabilities in the (positive-parity) ground states of  $^{29-31}\text{Na}$ . (d) Energies of the  $2p2h$ - and  $1p1h$ -dominant lowest states of  $^{30}\text{Na}$  (denoted by "2p2h" and "1p1h", respectively) measured from that of the  $0p0h$ -dominant lowest state. The range of the shell gap giving the  $n=0, 1, 2$  ground state ( $n$  ex) is indicated by  $n$  ex. Note that the corresponding shell gaps of  $^{29,31}\text{Na}$  are, respectively, smaller and larger by 0.24 MeV than the one of  $^{30}\text{Na}$ .

A larger  $x$  means primarily a lower neutron  $0d_{3/2}$  level, i.e., a wider  $N = 20$  gap in  $^{30}\text{Na}$ . Other effects are minor in this nucleus.

Figure 6 presents the variation of the ground-state properties of Na isotopes as a function of the gap thus varied. Results are mainly about  $^{30}\text{Na}$  unless otherwise specified. The SDPF-M interaction (at  $x = 0$ ) gives a narrow  $N = 20$  shell gap, i.e., 3.3 MeV for  $^{30}\text{Na}$ . As  $x$  is increased, the gap becomes wider, and the  $^{40}\text{Ca}$  gap ( $\sim 6$  MeV) is given by  $x \sim 2.6$ . An intermediate value  $x = 1$

reproduces the gap of USD ( $\sim 4.3$  MeV), implying that the USD includes some fractional effects of the current shell evolution [15].

The quadrupole moment and the magnetic moment in Fig. 6 (a) and (b) are almost constant up to the gap  $\sim 4$  MeV, as  $x$  is increased from 0. But, it jumps to values comparable to that of the USD model around the 4 MeV gap. In order to see how this rapid transition occurs, Fig. 6 (c) shows the probability of the intruder configurations in the lowest positive-parity state for  $^{30}\text{Na}$ . As expected from the change of the moments, the dominant component of the ground state moves rapidly from intruder to normal configurations at the shell gap  $\sim 4$  MeV.

It is interesting to compare this transition in  $^{30}\text{Na}$  with the ones of  $^{29,31}\text{Na}$  shown in Fig. 6 (c). Compared to the pattern of  $^{30}\text{Na}$ , notable differences are that (i) the shell gap causing the transition is larger in  $^{31}\text{Na}$  ( $\sim 5$  MeV) and smaller in  $^{29}\text{Na}$  ( $\sim 3$  MeV), and (ii) the transition takes place more slowly than  $^{30}\text{Na}$ . The former is because of the difference of the correlation energies in the normal states of  $^{29-31}\text{Na}$  discussed already, and the latter is because even- $N$  configurations are strongly connected with the pair-excited states via the pairing interaction. This is the reason why the intruder dominance in  $^{30}\text{Na}$  has a particular importance to clarify the shell structure of Na isotopes, and we now confirm that the narrower shell gap due to the shell evolution [15] plays a crucial role. Note that at the gap of stable nuclei ( $\sim 6$  MeV) the intruder dominance does not occur even in  $^{31}\text{Na}$ .

We finally discuss the competition of the dominant configurations in  $^{30}\text{Na}$  including a negative-parity state. Figure 6 (d) displays the energies of the  $2p2h$ - and  $1p1h$ -dominant lowest states measured from the energy of the  $0p0h$ -dominant state, as the gap is changed. In Fig. 4, we can see what happens as  $x$  is increased from 0. The  $2_1^+$  state is close to the  $3_1^-$  but stays lower consistently with experiment. If the gap is made larger, the ground state is switched to a negative-parity state around at 3.5 MeV, and persists for a while. At a larger shell gap  $\sim 4.5$  MeV, a competition between a positive-parity state and a negative-parity one is encountered again, where the former is dominated by normal configurations. Finally, after this competition the normal-dominant ground state persists. The “island of inversion” picture [8] seems to correspond to the gap near the second competition (i.e., around 4.5 to 5 MeV): with the weak-coupling approximation, the  $1\hbar\omega$  and  $2\hbar\omega$  states were calculated to be located at 0.306 and 0.776 MeV above the normal one, respectively [8].

The competition of normal- and abnormal-parity states in  $^{30}\text{Na}$  ( $N = 19$ ) can be compared to a famous example of the parity inversion in  $^{11}\text{Be}$  ( $N = 7$ ). Both are related to the narrow shell gap, but we point out a

large difference between them: the latter is considered as the competition between the  $0p0h$  and  $1p1h$  states, corresponding to the second competition in the present paper. Thus, in the case of the  $N = 20$  region a more drastic event occurs in spite of the normal-parity ground state of  $^{30}\text{Na}$ , reflecting a further narrowing of the shell gap.

## VI. SUMMARY

In summary, we have investigated where the disappearance of the magic structure starts in the isotope chain of Na referring to its mechanism. It is suggested that experimental electromagnetic moments, energy levels, and  $B(E2)$  values of  $^{30}\text{Na}$  with  $N = 19$  clearly indicate the dominance of the intruder configurations in its ground state, by combining with a shell-model calculation using the MCSM. The present result is in sharp contrast to a previous speculation based on the USD model [7] from the viewpoint of the binding energy, where the disappearance was supposed to occur right at  $N = 20$ . The same conclusion as this speculation was drawn by the “island of inversion” model. The difference between the present calculation and the previous models is mainly in the behavior of the effective  $N = 20$  shell gap for small  $Z$ : the gap is substantially narrow (about 3 MeV) for Na isotopes with the present SDPF-M interaction. Nevertheless, owing to the monopole part of the SDPF-M interaction, in particular, its spin-isospin dependent component, the well-known 6 MeV gap is restored for  $^{40}\text{Ca}$ , as an example of the shell evolution in stable and unstable nuclei [15]. The validity of this argument has been confirmed in this study quite transparently with Na isotopes below  $N = 20$  where the intruder states are shown to be, most likely, unable to beat the normal states without a narrower shell gap.

## Acknowledgments

This work was supported mainly by Grant-in-Aid for Specially Promoted Research (13002001) from the MEXT, by the RIKEN-CNS collaboration project on large-scale nuclear structure calculation, and by the U.S. National Science Foundation under Grant No. PHY-0110253. One of the authors (Y.U.) is grateful to Dr. T. Shizuma for discussions about the collective property of odd-odd nuclei. He acknowledges the support in part by Grant-in-Aid for Young Scientists (14740176) from the MEXT, and the Helios computer system in JAERI. The conventional shell-model calculation was carried out by the code OXBASH [39].

[1] C. Thibault *et al.*, Phys. Rev. C **12**, 644 (1975).

[2] X. Campi, H. Flocard, A.K. Kerman, and S. Koonin,

Nucl. Phys. **A251**, 193 (1975).

[3] C. Détraz *et al.*, Phys. Rev. C **19**, 164 (1979).

[4] D. Guillemaud-Mueller *et al.*, Nucl. Phys. **A426**, 37 (1984).

[5] T. Motobayashi *et al.*, Phys. Lett. B **346**, 9 (1995).

[6] Y. Yanagisawa *et al.*, Phys. Lett. B **566**, 84 (2003).

[7] B.A. Brown and B.H. Wildenthal, Annu. Rev. Nucl. Part. Sci. **38**, 29 (1988).

[8] E.K. Warburton, J.A. Becker, and B.A. Brown, Phys. Rev. C **41**, 1147 (1990).

[9] E. Caurier, F. Nowacki, A. Poves, and J. Retamosa, Phys. Rev. C **58**, 2033 (1998).

[10] For a review, T. Otsuka, M. Honma, T. Mizusaki, N. Shimizu, and Y. Utsuno, Prog. Part. Nucl. Phys. **47**, 319 (2001).

[11] Y. Utsuno, T. Otsuka, T. Mizusaki, and M. Honma, Phys. Rev. C **60**, 054315 (1999).

[12] Y. Utsuno, T. Otsuka, T. Mizusaki, and M. Honma, Phys. Rev. C **64**, 011301(R) (2001).

[13] T.T.S. Kuo and G.E. Brown, Nucl. Phys. **A114**, 241 (1968).

[14] D.J. Millener and D. Kurath, Nucl. Phys. **A255**, 315 (1975).

[15] T. Otsuka, R. Fujimoto, Y. Utsuno, B.A. Brown, M. Honma, and T. Mizusaki, Phys. Rev. Lett. **87**, 082502 (2001).

[16] D. Guillemaud-Mueller *et al.*, Phys. Rev. C **41**, 937 (1990).

[17] M. Fauerbach *et al.*, Phys. Rev. C **53**, 647 (1996).

[18] O. Tarasov *et al.*, Phys. Lett. B **409**, 64 (1997).

[19] H. Sakurai *et al.*, Phys. Lett. B **448**, 180 (1999).

[20] A. Ozawa, T. Kobayashi, T. Suzuki, K. Yoshida, and I. Tanihata, Phys. Rev. Lett. **84**, 5493 (2000).

[21] D. Lunney *et al.*, Phys. Rev. C **64**, 054311 (2001).

[22] M. Keim, in *Proceeding of the International Conference on Exotic Nuclei and Atomic Masses (ENAM98)*, edited by B.M. Sherrill, D.J. Morrissey, and C.N. Davis, AIP Conf. Proc. **455**, p.50 (AIP, New York, 1998).

[23] M. Keim *et al.*, Euro. Phys. J. A **8**, 31 (2000).

[24] B.V. Pritychenko *et al.*, Phys. Rev. C **63**, 011305(R) (2001).

[25] B.V. Pritychenko *et al.*, Phys. Rev. C **66**, 024325 (2002).

[26] M. Honma, T. Mizusaki, and T. Otsuka, Phys. Rev. Lett. **75**, 1284 (1995).

[27] T. Mizusaki, M. Honma, and T. Otsuka, Phys. Rev. C **53**, 2786 (1996).

[28] M. Honma, T. Mizusaki, and T. Otsuka, Phys. Rev. Lett. **77**, 3315 (1996).

[29] T. Otsuka, M. Honma, and T. Mizusaki, Phys. Rev. Lett. **81**, 1588 (1998).

[30] B.A. Brown and B.H. Wildenthal, Nucl. Phys. **A474**, 290 (1987).

[31] M. Honma, T. Otsuka, B.A. Brown, and T. Mizusaki, Phys. Rev. C **69**, 034335 (2004).

[32] M. Honma, T. Otsuka, B.A. Brown, and T. Mizusaki, Phys. Rev. C **65**, 061301(R) (2002).

[33] G. Huber *et al.*, Phys. Rev. C **18**, 2342 (1978).

[34] G. Audi, O. Bersillon, J. Blachot, and A.H. Wapstra, Nucl. Phys. **A624**, 1 (1997).

[35] N. Fukunishi, T. Otsuka, T. Sebe, Phys. Lett. B **296**, 279 (1992).

[36] M.W. Cooper *et al.*, Phys. Rev. C **65**, 051302(R) (2002).

[37] P. Baumann *et al.*, Phys. Rev. C **36**, 765 (1987).

[38] C.J. Gallagher, Jr. and S.A. Moszkowski, Phys. Rev. **111**, 1282 (1958).

[39] B.A. Brown, A. Etchegoyen, W.D.M. Rae, MSU-NSCL Report No. 524 (1986).